Acta Oceanol. Sin., 2024, Vol. 43, No. 9, P. 54–69
https://doi.org/10.1007/s13131-024-2361-4
http://www.aosocean.com
E-mail: ocean2@hyxb.org.cn

Corrections of shipboard GPS radiosonde soundings and applications on historical records in the eastern tropical Indian Ocean and South China Sea

Zewen Wu[1, 2], Xin Liu[1, 3], Yunkai He[1], Haoyu Jiang[2], Bo Peng[4]*, Ke Huang[1, 5]*

[1] State Key Laboratory of Tropical Oceanography, South China Sea Institute of Oceanology, Chinese Academy of Sciences, Guangzhou 510301, China

[2] Hubei Key Laboratory of Marine Geological Resources, China University of Geosciences, Wuhan 430074, China

[3] Guangzhou Cigarette Factory of China Tobacco Guangdong Industrial Co., Ltd., Guangzhou 510385, China

[4] Institute for Environmental and Climate Research, Jinan University, Guangzhou 511443, China

[5] Fujian Provincial Key Laboratory of Marine Physical and Geological Processes, Xiamen 361000, China

Received 19 April 2024; accepted 17 June 2024

Abstract

Shipboard radiosonde soundings are important for detecting and quantifying the multiscale variability of atmosphere-ocean interactions associated with mass exchanges. This study evaluated the accuracies of shipboard Global Positioning System (GPS) soundings in the eastern tropical Indian Ocean and South China Sea through a simultaneous balloon-borne inter-comparison of different radiosonde types. Our results indicate that the temperature and relative humidity (RH) measurements of GPS-TanKong (GPS-TK) radiosonde (used at most stations before 2012) have larger biases than those of ChangFeng-06-A (CF-06-A) radiosonde (widely used in current observation) when compared to reference data from Vaisala RS92-SGP radiosonde, with a warm bias of 5℃ and dry bias of 10% during daytimes, and a cooling bias of –0.8℃ and a moist bias of 6% during nighttime. These systematic biases are primarily attributed to the radiation effects and altitude deviation. An empirical correction algorithm was developed to retrieve the atmospheric temperature and RH profiles. The corrected profiles agree well with that of RS92-SGP, except for uncertainties of CF-06-A in the stratosphere. These correction algorithms were applied to the GPS-TK historical sounding records, reducing biases in the corrected temperature and RH profiles when compared to radio occultation data. The correction of GPS-TK historical records illustrated an improvement in capturing the marine atmospheric structure, with more accurate atmospheric boundary layer height, convective available potential energy, and convective inhibition in the tropical ocean. This study contributes significantly to improving the quality of GPS radiosonde soundings and promotes the sharing of observation in the eastern tropical Indian Ocean and South China Sea.

Key words: shipboard GPS radiosonde soundings, corrections, temperature, relative humidity, eastern tropical Indian Ocean, South China Sea

Citation: Wu Zewen, Liu Xin, He Yunkai, Jiang Haoyu, Peng Bo, Huang Ke. 2024. Corrections of shipboard GPS radiosonde soundings and applications on historical records in the eastern tropical Indian Ocean and South China Sea. Acta Oceanologica Sinica, 43(9): 54–69, doi: 10.1007/s13131-024-2361-4

1 Introduction

Observational vertical profiles of atmospheric temperature, relative humidity (RH) and pressure are crucial for exploring the atmospheric boundary layer, validating the ground-based and satellite remote sensor retrievals, investigating the synoptic-scale low-level westerly and upper-level easterly wind bursts (which are commonly associated with El Niño events) (Eisenman et al., 2005), and developing water vapor and cloud parameterizations in atmospheric models (e.g., Meehl, 1997; Luers and Eskridge, 1998; Vömel et al., 2002; Seidel et al., 2004; Kuo et al., 2005; Baldwin et al., 2001; Durre et al., 2006; Yu et al., 2009; Wang et al., 2010, 2014; Qin et al., 2012; Cheng et al., 2015; Chang et al., 2018; Zhang et al., 2019). These vertical records have been primarily provided by balloon-borne radiosonde sensors for more than 50 years (Luers and Eskridge, 1998). The compilations of such ground-based records are worldwide available, e.g., the Integrated Global Radiosonde Archive (IGRA), the World Meteorological Organization (WMO) standard upper-air observatory dataset, and the National Weather Service Archive (NWSA). Nevertheless, there were sparse sounding records and associated ap-

Foundation item: The Second Tibetan Plateau Scientific Expedition and Research Program under contract No. 2019QZKK0102-02; the National Natural Science Foundation of China under contract Nos 42230402, 92158204, 42176026, 42076201, 41049903, 41149908, 41249906, 41249907, and 41249910; the Guangdong Basic and Applied Basic Research Foundation under contract No. 2022A1515240069; the Marine Economic Development Special Program of Guangdong Province (Six Major Marine Industries): Research and Demonstration of Critical Technologies for Comprehensive Prevention and Control of Natural Disaster in Offshore Wind Farms, China under contract No. 29[2023]; the Fund of Fujian Provincial Key Laboratory of Marine Physical and Geological Processes under contract No. KLMPG-22-02.

*Corresponding author, E-mail: pengbo@jnu.edu.cn; kehuang@scsio.ac.cn

plications in the Eastern Tropical Indian Ocean (ETIO) and the South China Sea (SCS), to some extent limiting the investigations of atmosphere-ocean interaction in these regions (Wang et al., 2010, 2019; Xie et al., 2014; Peng et al., 2016; Shi et al., 2017).

In recent decades, large amounts of Global Positioning System (GPS) soundings have been deployed over the ETIO and SCS covering the period from 2006 to present by the South China Sea Institute of Oceanology (SCSIO), Chinese Academy of Sciences, China (Fig. 1). However, as will be discussed later, 711 sounding historical records of first-generation sea-based radiosonde (used at most stations before 2012) have suffered from significant systematic biases in temperature and RH measurements. The use of these sea-based historic radiosonde records in climate studies and atmospheric reanalysis has been seriously hindered by their inhomogeneity due to the upgrades in instrument type, observational practice, or other issues (Zhai and Eskridge, 1996). Quantifying error sources in radiosonde records and making associated corrections are urgently needed. It is important to note that the Radio Occultation (RO) data could be affected by cloud biases and algorithm errors (Zou and Tian, 2018; Zou et al., 2019; Tian and Zou, 2020), with errors of around 1 ℃ from the surface to about 40 km (Angling, 2016). Globally, due to the errors/uncertainties caused by instrumentation displacement (e.g., inconsistent reference frame, antenna phase variations, irradiation coating technology and hardware changes), there have been plenty of studies focusing on quantifying and correcting the temperature and RH biases for different types of radiosondes and significantly improving their applications, especially for Vaisala radiosondes like Vaisala RS80, RS90, and RS92 (e.g., Miloshevich et al., 2001; Wang et al., 2002; Zhang et al., 2019).

Simultaneous balloon-borne inter-comparison provides an efficient way to identify the error sources for different radiosondes types (Suortti et al., 2008; Sinha et al., 2016). Previous radiosonde inter-comparison campaigns, especially those organized by the WMO, have been instrumental in assessing the accuracy and diversity of widely used operational radiosonde types (e.g., Hooper, 1986; Nash and Schmidlin, 1987; Schmidlin, 1988; Ivanov et al., 1991; Yagi et al., 1996; Nash et al., 2006; Balagurov et al., 2006; Da Silveira et al., 2006). Especially, the 8th international radiosonde inter-comparison, performed in Yangjiang, China, during July 12 to August 3, 2010 (Nash et al., 2011; Li et al., 2011), have assessed the capability of the Vaisala RS92 radiosondes and suggested that Vaisala RS92-SGP has high level of accuracy and consistency (Jauhiainen and Lehmuskero, 2005), can provide a simultaneous reference for the inter-comparison campaigns (Luers, 1997; Nash et al., 2011; Li et al., 2011). In this study, the systematic errors of the sea-based GPS radiosondes over the ETIO and SCS are evaluated through simultaneous inter-comparison with the Vaisala RS92-SGP, and empirical corrections were applied to the historical radiosonde records.

The simultaneous GPS sounding inter-comparison was conducted during the R/V *ShiYan 1* in the spring of 2012, comprising 20 balloon-borne radiosonde flights for Vaisala RS92-SGP, Beijing GPS-TK and Changfeng CF-06-A. The subsequent sections of this study is organized as follows. Section 2 describes the GPS radiosonde systems and data. Section 3 presents the results of the radiosonde-based biases. Correction models will then be developed in Section 4. In Section 5, the historical radiosonde records will be corrected and validated, followed by the summary and discussion in Section 6.

2 Materials and methods

2.1 *GPS-TanKong (GPS-TK) radiosonde system*

The GPS-TK radiosonde is the first-generation Chinese sea-based upper-air sounding system designed by the Key Laboratory of Middle Atmosphere and Global Environment Observation (LAGEO) of the Institute of Atmospheric Physics (IAP), China. It was used for low-layer atmospheric measurement and consists of a ground system, antenna, and radiosonde. The radiosonde is equipped with a cylindrical rod thermistor temperature sensor, a planar thin-film humicap humidity sensor and GPS positioning system to obtain temperature, RH and altitude profiles, respectively. The rod temperature sensor in the GPS-TK radiosonde has a bigger size and slower response compared to the thin wire capacitor of CF-06-A and Vaisala RS92-SGP, which could lead to temperature biases due to solar and infrared radiation heating/cooling and the time lag of the sensor in responding to temperature gradients (Mcinturuff et al., 1979). The production calibration of the GPS-TK relies on the basic humidity calibration model and also partly on linear temperature dependence calculation modeling, potentially resulting in a dry bias in RH measure-

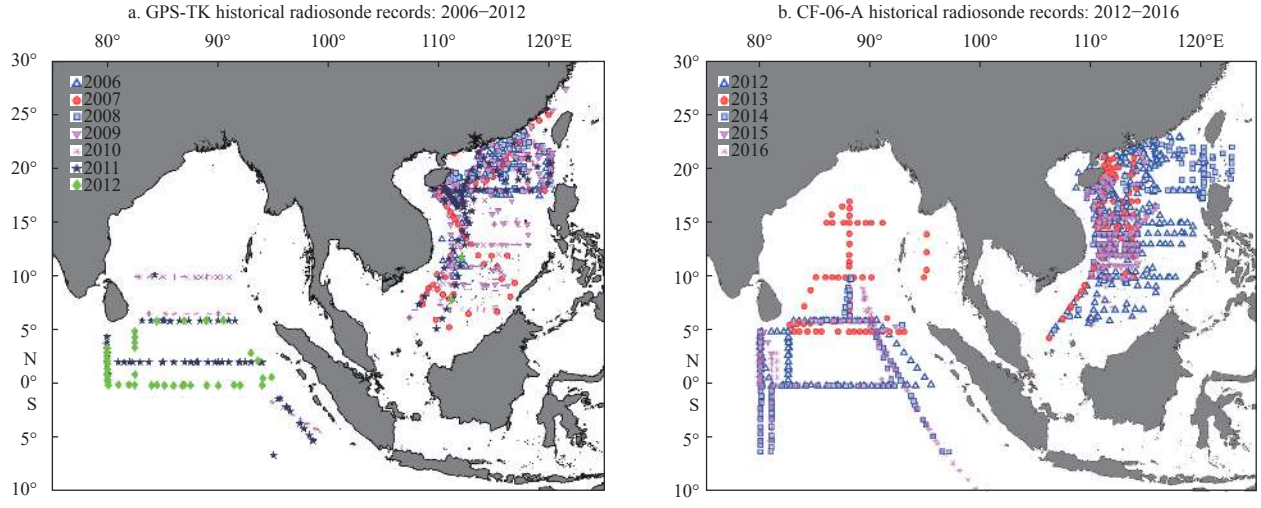

Fig. 1. Geographical maps of GPS-TK (a) and CF-06-A (b) historical radiosonde records over the ETIO and SCS. Colored symbols represent the various years when the datasets were collected.

ments under cold and humid conditions (Wang et al., 2002). Additionally, the GPS-TK radiosonde lacks a pressure sensor, and its pressure profiles are reconstructed from temperature, RH and altitude profiles derived from the sounding (refer to Appendix for details).

2.2 *ChangFeng-06-A (CF-06-A) radiosonde system*

The CF-06-A is a new-generation China sea-based sounding system developed by Beijing Changfeng Micro-electronics Technology Co. (CFMTC), Ltd., China, which consists of CF-GPS-JS receiving system, ground check kit, antenna and radiosonde. The CF-GPS-JS system is responsible for receiving ground-based positioning information, tracking and demodulating radiosonde transmission signals, and transmitting meteorological and positioning information back to the terminal computer for data processing. The radiosonde of CF-06-A includes a bead resistance temperature sensor known for its good radiation characteristics and a high sensitivity, along with a thin-film capacitors humidity sensor from Sweden manufacturers. The 8th WMO international inter-comparison has confirmed that CF-06-A can provide high-quality pressure, temperature, humidity, and wind measurements with proper error correction (Nash et al., 2011). However, it's important to note that these WMO inter-comparisons were conducted based on land releases, which may not fully represent conditions at sea.

2.3 *Vaisala RS92-SGP radiosonde system*

The Vaisala RS92-SGP originates from the Finland. The main system of Vaisala includes a processor (Vaisala, DigiCORA III), GPS antenna (GA20), UHF antenna (RB21), ground check kit (GC25), balloon launcher (ASAP), and GPS radiosonde sensor (RS92-SGP). The all-digital RS92-SGP, equipped with the newest Vaisala, Ltd. radiosonde model, has been widely used since 2005 (Jauhiainen and Lehmuskero, 2005). It features capacitive wire temperature sensors and thin film capacitor-heated twin humidity sensors, and incorporates a reconditioning method to completely remove chemical contamination using the ground check kit. Table 1 shows the details of these three radiosondes.

Table 1. Characteristics of GPS-TK, CF-06-A, and RS92-SGP radiosonde systems (updated table of Xie et al., 2014)

Radiosonde	Manufacturer and country	Temperature sensor	Humidity sensor	Digital frequency specification	Anti-radiation coating	Weight/g
GPS-TK	LAGEO, IAP, Beijing (China)	band-gap thermistor: type SHT 10, range from –40℃ to +125℃, resolution 0.04℃, response time 5 s, uncertainty N/A, area 4.94 mm × 7.47 mm, software adjustment, no	polymer capacitive: type SHT 10, range from 0% to 100%RH, resolution 0.4% RH, response time 8 s, uncertainty N/A, area 4.94 mm × 7.47 mm, software adjustment, no	range from 400 MHz to 406 MHz, tuning N/A, stability N/A, R/S power N/A	no aluminised	150
CF-06-A	Beijing Changfeng Micro-electronics Technology Co. (China)	bead thermistor: type MF51MP, range from –90℃ to +60℃, resolution 0.1℃, response time 0.8 s, uncertainty 0.5℃, diameter 0.8 mm, software adjustment, yes	thin-film capacitor: type Sweden XC06, range from 0% to 100 % RH, resolution 1 % RH, response time 1.5 s, uncertainty 5% RH, area 3.8 mm × 5 mm, software adjustment, no	range from 400 MHz to 406 MHz, tuning, any in range, stability +/– 10 kHz, R/S power 100 mW	space micro-process anti-radiation technology, aluminized, protective cap	270
RS92-SGP	Vaisala, Ltd. (Finland)	thin wire capacitor: range from –90℃ to +60℃, resolution 0.1℃, response time 0.4 s, uncertainty 0.2℃, diameter 0.5 mm, software adjustment, yes	thin-film capacitor, heated twin sensor (polymer for low RH): type RD100, range from 0%–100% RH, resolution 1% RH, response time 0.5 s, uncertainty 2% RH, area 2.5 mm × 2.5 mm, software adjustment, yes	range from 400 MHz to 406 MHz, tuning 10 kHz, stability +/– 2 kHz, R/S power 60 mW	reflectivity coating, aluminized, shiny silver	290

Note: R/S, root mean square power; N/A, not available.

Table 2. Details of 20 simultaneous balloon-borne radiosonde flights over the ETIO

No.	Longitude	Latitude	Local time	Day/night	No.	Longitude	Latitude	Local time	Day/night
1*	**111.092°E**	**7.860°N**	**Feb. 28, 14:00**	**day**	11	82.504°E	3.485°S	Mar. 20, 20:00	night
2	**90.483°E**	**6.009°N**	**Mar. 10, 18:00**	**day**	**12**	**82.535°E**	**4.474°S**	**Mar. 21, 08:00**	**day**
3	90.462°E	6.050°N	Mar. 11, 00:00	night	13	80.080°E	4.989°S	Mar. 22, 20:00	night
4	89.003°E	5.993°N	Mar. 11, 20:00	night	**14**	**80.003°E**	**3.494°S**	**Mar. 23, 14:00**	**day**
5	86.995°E	6.020°N	Mar. 13, 20:00	night	15	80.014°E	2.995°S	Mar. 23, 20:00	night
6	84.497°E	5.964°N	Mar. 15, 20:00	night	16	80.090°E	0.494°S	Mar. 25, 02:00	night
7	82.469°E	6.001°N	Mar. 16, 19:00	night	**17**	**80.132°E**	**0.017°S**	**Mar. 25, 14:00**	**day**
8	82.535°E	0.943°N	Mar. 18, 20:00	night	18	80.049°E	0.492°N	Mar. 25, 20:00	night
9	82.508°E	0.009°S	Mar. 19, 02:00	night	19	84.009°E	0.026°N	Apr. 04, 19:00	night
10	82.544°E	1.454°S	Mar. 19, 20:00	night	**20**	**86.002°E**	**0.003°N**	**Apr. 05, 14:00**	**day**

Note: Bold font represents the daytime flights and unbold font represents the nighttime flights. Symbol * represents the missing of RS92-SGP measurement. Local time format: month day, hour (UTC+6).

2.4 *Dataset of simultaneous inter-comparison soundings*

The simultaneous high vertical resolution measurements derived from the GPS radiosondes comprised 14 nighttime flights and 6 daytime flights (Table 2, one RS92-SGP daytime sounding missing). During each balloon flights, the three GPS radiosondes were suspended using a wire approximately 8 m in length, positioned near the tail and separated from each other by 1 m. Meteorological parameter Measurements were taken with a time resolution of 2 s. Altitude derived from GPS was used as the vertical coordinate. Figures 2a–d depict two examples of simultaneous temperature and RH measurements from RS92-SGP, CF-06-A and GPS-TK, illustrating the common characteristics of daytime and nighttime flights. Figure 2e provides a schematic detailing the connection of radiosondes and the balloon during the simultaneous inter-comparison soundings.

2.5 *COSMIC RO dataset*

The Constellation Observing System for Meteorology, Ionosphere and Climate (COSMIC) RO provides approximately 2 500 atmospheric profiles every day within a height range of 0.1–40 km around the world. The profiles are provided with 100-m vertical resolution, although the actual resolution is a function of height and is about 1 km in the tropical tropopause transition layer. The National Center for Atmospheric Research (NCAR) has made available COSMIC profiles corrected for the effects of water vapor on the GPS signal. Further details regarding COSMIC-derived temperature and RH measurements could be found in Ho et al. (2009), He et al. (2009), and Yunck et al. (2009).

3 Results

3.1 *Significant biases in historical GPS sounding records*

During 2006–2011 ETIO and SCS cruise experiments of GPS-TK observation stage, 711 historical sounding records were conducted by SCSIO. Temperature and RH soundings using the GPS-TK radiosonde were conducted every 6 h during this stage. Comparisons were made between collocated tropical ocean atmospheric temperature and RH profiles from historical GPS-TK radiosondes and from COSMIC to assess the accuracy of GPS-TK soundings. Note that the collocation of COSMIC is within 3 h and 400 km by comparing to the shipboard sounding locations. Figure 3 illustrates the relative differences of temperature and RH between GPS-TK and COSMIC RO as a function of altitude height for 45 daytime and 36 nighttime collocation cases. The temperature biases in the low-level troposphere were estimated to be around 8℃ during daytime (Figs 3a and b) and around 3℃ during nighttime (Figs 3c and d), while RH biases were found to be between 10% to 40% for dry biases when comparing with the satellite RO of COSMIC. These results indicate warm temperature and dry RH biases in GPS-TK historical sounding records compared to valuable reference data, particularly in daytime, suggesting that the temperature and RH biases derived from GPS-TK radiosondes found in Fig. 3 are attributed to the influence of solar radiation as discussed by Vömel et al. (2007) and Yoneyama et al. (2008).

3.2 *Temperature and RH biases derived from simultaneous inter-comparison*

3.2.1 *Biases in temperature profiles*

The temperature profiles of GPS-TK and CF-06-A and their differences with RS92-SGP are shown in Fig. 4. The temperature biases between GPS-TK and RS92-SGP vary significantly over the LT both during daytime and nighttime (Figs 4a and e). The mean biases of GPS-TK exceed 2℃ at most altitudes with a maximum difference of up to 6℃ and a predominant Root Mean Square (RMS) difference of 0.6℃ in the troposphere during the daytime. These significant biases of GPS-TK are mainly attributed to solar radiation heating. Anomalously large biases also appeared dur-

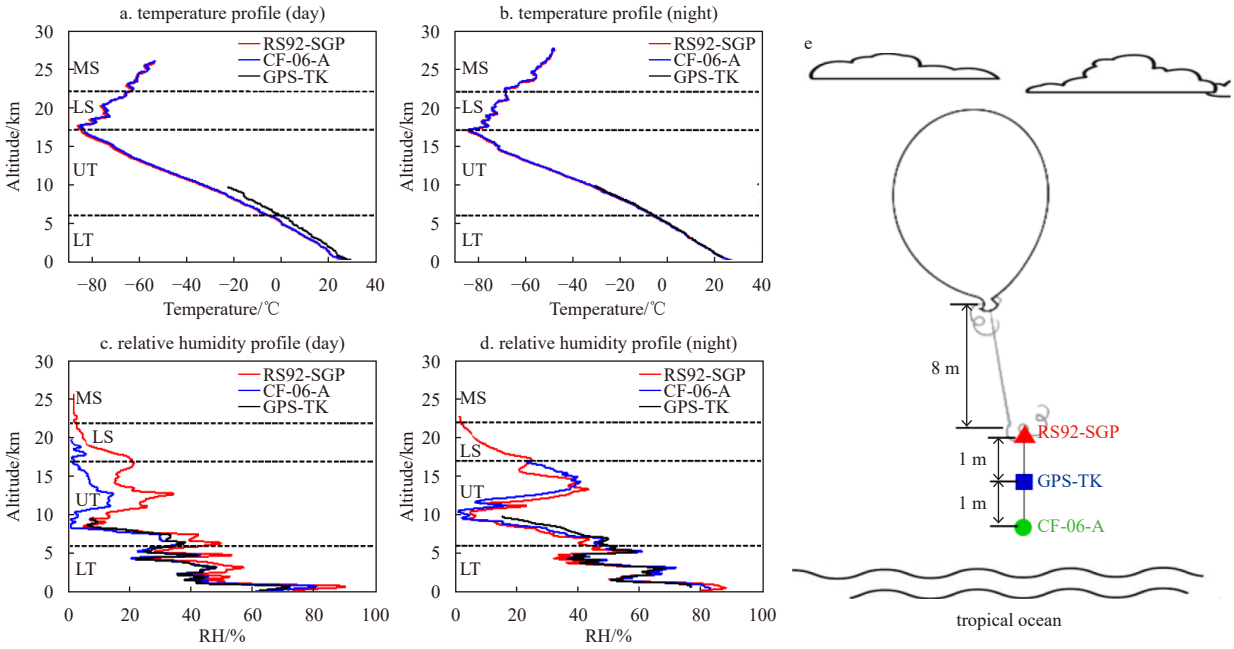

Fig. 2. Temperature (a) and RH (c) profiles of RS92-SGP (red), CF-06-A (blue) and GPS-TK (black) launched at (0°N, 86°E) at 13:33, 5 April 2012; temperature (b) and RH (d) profiles launched at (0.026°N, 84°E) at 19:38, 4 April 2012; schematic on the simultaneous inter-comparison soundings (e). MS: middle stratosphere; LS: lower stratosphere; UT: upper troposphere; LT: lower troposphere.

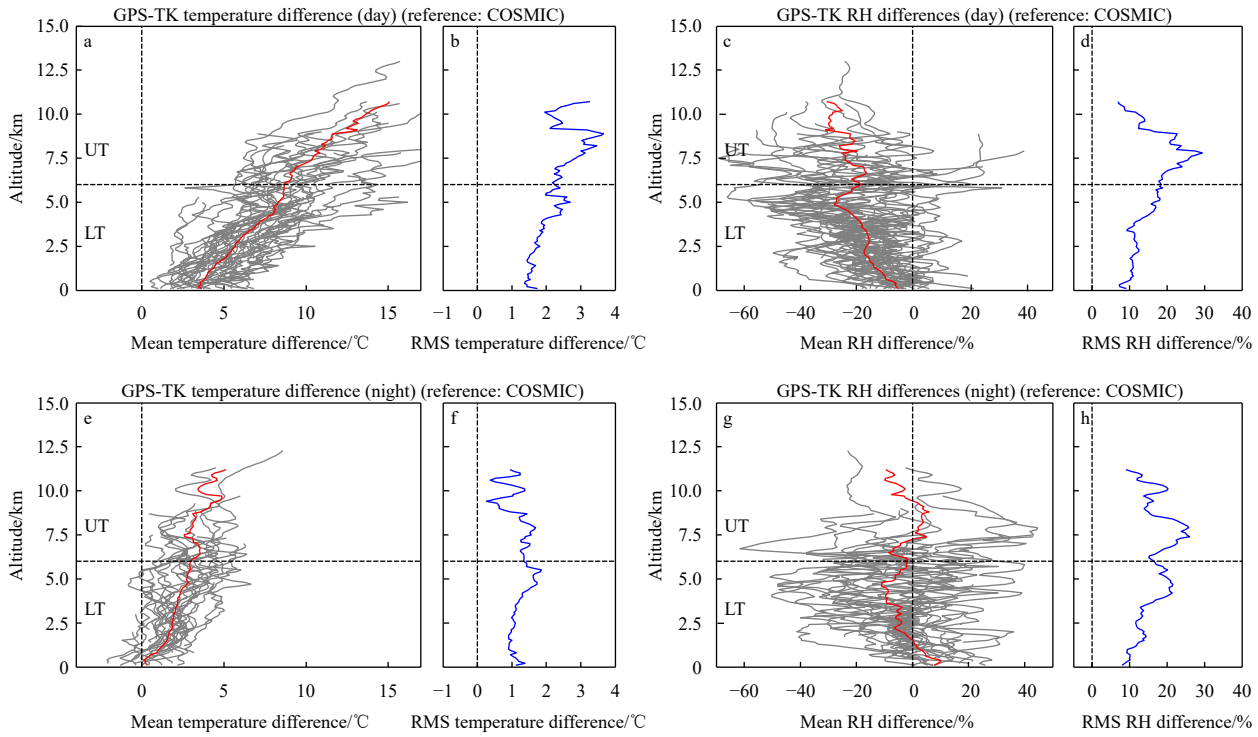

Fig. 3. Comparisons of GPS-TK radiosonde with COSMIC: mean (red) (a) and Root Mean Square (RMS) (blue) (b) of GPS-TK temperature difference in daytime; comparisons of GPS-TK radiosonde with COSMIC: mean (red) (c) and RMS (blue) (d) of GPS-TK RH difference in daytime; comparisons of GPS-TK radiosonde with COSMIC: mean (red) (e) and RMS (blue) (f) of GPS-TK temperature difference in nighttime; comparisons of GPS-TK radiosonde with COSMIC: mean (red) (g) and RMS (blue) (h) of GPS-TK RH difference in nighttime. The collocation of COSMIC is within 3 h and 400 km. Gray lines: individual GPS-TK difference. Gray lines in a, c, e, and g are the individual temperature differences for each inter-comparison. UT: upper troposphere; LT: lower troposphere.

ing the nighttime. The GPS-TK shows a cold bias of –0.8℃, with a RMS difference of 0.8℃ below 10 km. Such nighttime biases are believed to result from the inadequate treatment of long-wave radiation cooling.

The relative systematic error of CF-06-A radiosonde is within 0.4℃ and the standard deviation is within 0.7℃ in the 8th WMO inter-comparison (Nash et al., 2011; Li et al., 2011). In our inter-comparison, the mean temperature biases of CF-06-A during day-time flights show slightly warm biases, increasing continuously with altitude from zero to 1.5℃ below 17 km (Fig. 4c), indicating that temperature correction model is inflexible and the solar heating is insufficiently corrected during the daytime. During the nighttime flights, the CF-06-A shows a cool bias of –0.5℃ in the lower troposphere (below 12 km), and these differences decrease significantly with altitude, turning into a warm bias of 0.4℃ around 17 km (Fig. 4g). This might be due to the overcorrection of radiation cooling biases. The RMS of the CF-06-A typically consists of a nearly constant value in the range of 0.1–0.2℃ during daytime and 0.2–0.3℃ during nighttime below 17 km (Figs 4d and h). These relative homogeneous curves indicate that the error characteristics of CF-06-A are insensitive with altitudes below 17 km both during daytime and nighttime. Above 17 km, the error characteristics became more complicated, with a large RMS difference of 1℃. These phenomena indicate that the temperature correction models of the CF-06-A become disoriented in strong temperature inversion environments.

3.2.2 *Biases in RH profiles*

As noted by Wang et al. (2002), the temperature-dependence errors are among the most important contributors to the total RH errors in radiosonde measurements. Figure 5 shows the mean RH biases of the GPS-TK and CF-06-A compared to RS92-SGP during daytime and nighttime flights. The GPS-TK exhibits a dry mean bias of 10% over the troposphere during daytime and a moist bias of 6% during nighttime from the lower to upper troposphere (Figs 5a and e). The RMS of the GPS-TK contains large variations in the range of 5%–8% during daytime and a consistent 4% during nighttime, indicating that the RH sensor has a poor response to humidity changes in warm temperature environments. The dry biases in radiosonde humidity profiles can lead to severe underestimation of convective available potential energy and overestimation of convective inhibition (Guichard et al., 2000). The comparison of RH data between L-band and 59–701 sounding system of Yao et al. (2017) revealed that the RH bias is related not only to ambient temperature change, but also to RH changes, reflecting the possible “wet hysteresis loop” effect of humidity sensors.

During the 8th WMO inter-comparison, the RH measurements of CF-06-A basically showed a dry trend compared to the Vaisala radiosonde, with 4% below 14 km and 12 % above 14 km (Li et al., 2011). Additionally, the Vaisala radiosondes were found to have a calibration-based dry bias (Miloshevich et al., 2001) or a contamination dry bias (Wang et al., 2002). In our inter-comparison, the RH mean biases for the CF-06-A measurements show a dry bias of 4% during daytime (Fig. 5c) and a moist bias ranging from 4% to 8% during nighttime (Fig. 5g) throughout the troposphere, indicating good consistency within the diurnal variation. It approves the fact that the CF-06-A is equipped with equivalent sensors of the twin H-Humicap with an aluminized plastic shield (CF GPS radiosonde system, 2009). The RMS of the CF-06-A

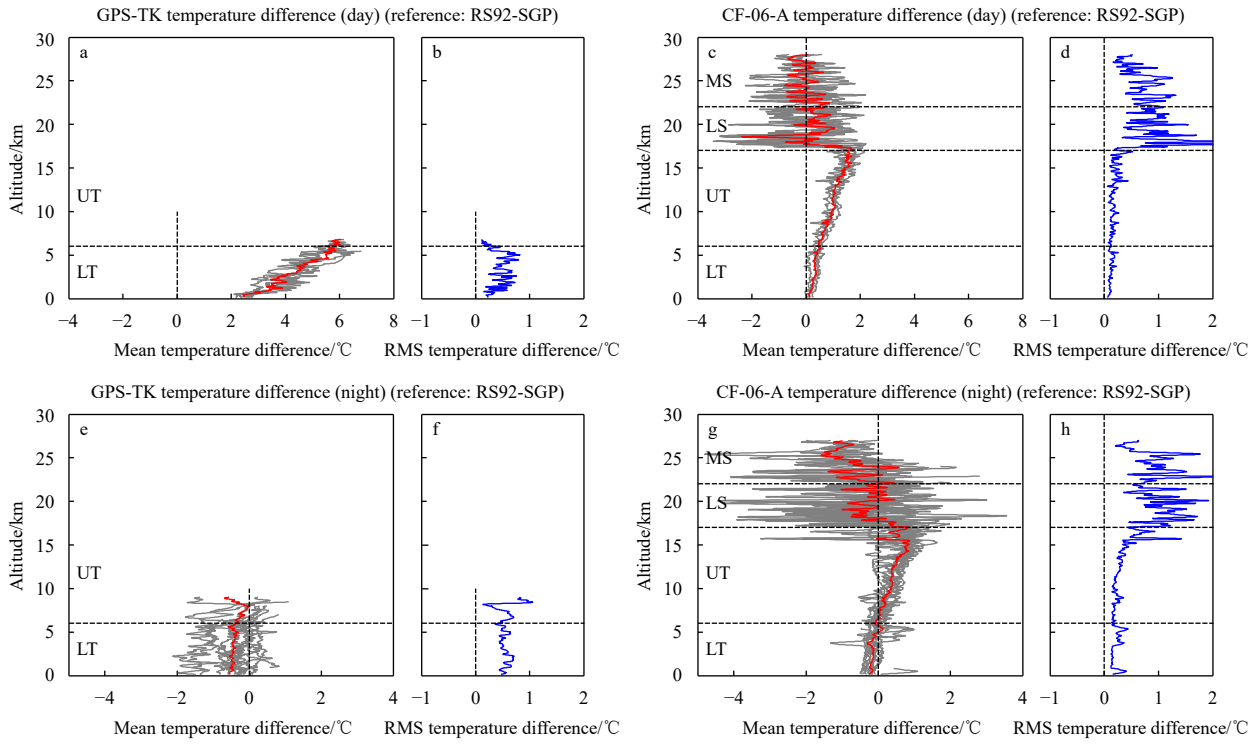

Fig. 4. Mean (a) and Root Mean Square (RMS) (b) of GPS-TK temperature differences in daytime; mean (c) and RMS (d) of CF-06-A temperature differences in daytime; mean (e) and RMS (f) of GPS-TK temperature differences in nighttime; mean (g) and RMS (h) of CF-06-A temperature differences in nighttime. Red lines: mean biases; gray lines: individual differences; blue lines: RMS. Gray lines in a, c, e, and g are the individual temperature differences for each inter-comparison. LT: lower troposphere; UT: upper troposphere; LS: lower stratosphere; MS: middle stratosphere. Updated figure of Xie et al. (2014).

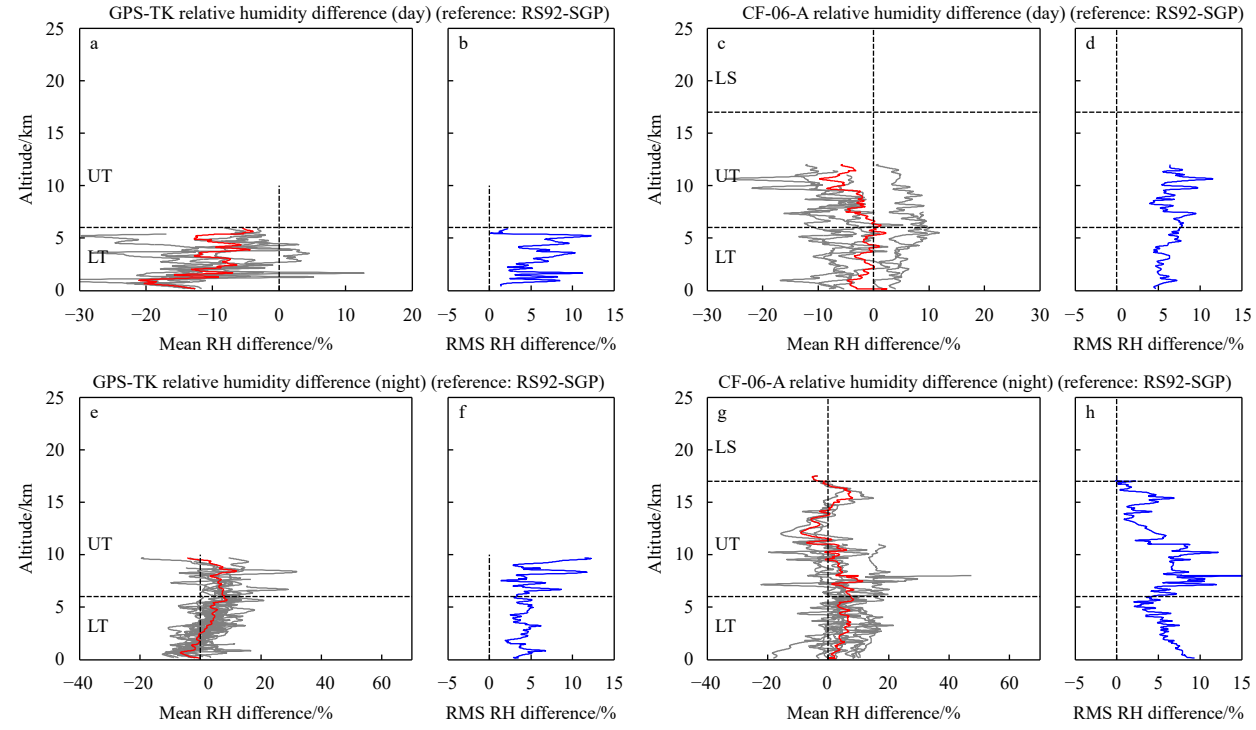

Fig. 5. Mean (a) and Root Mean Square (RMS) (b) of GPS-TK RH differences in daytime; mean (c) and RMS (d) of CF-06-A RH differences in daytime; mean (e) and RMS (f) of GPS-TK RH differences in nighttime; mean (g) and RMS (h) of CF-06-A RH differences in nighttime. Red lines: mean biases; gray lines: individual differences; blue lines: RMS. Gray lines in a, c, e, and g are the individual temperature differences for each inter-comparison. LS: lower stratosphere. UT: upper troposphere; LT: lower troposphere. Updated figure of Xie et al. (2014).

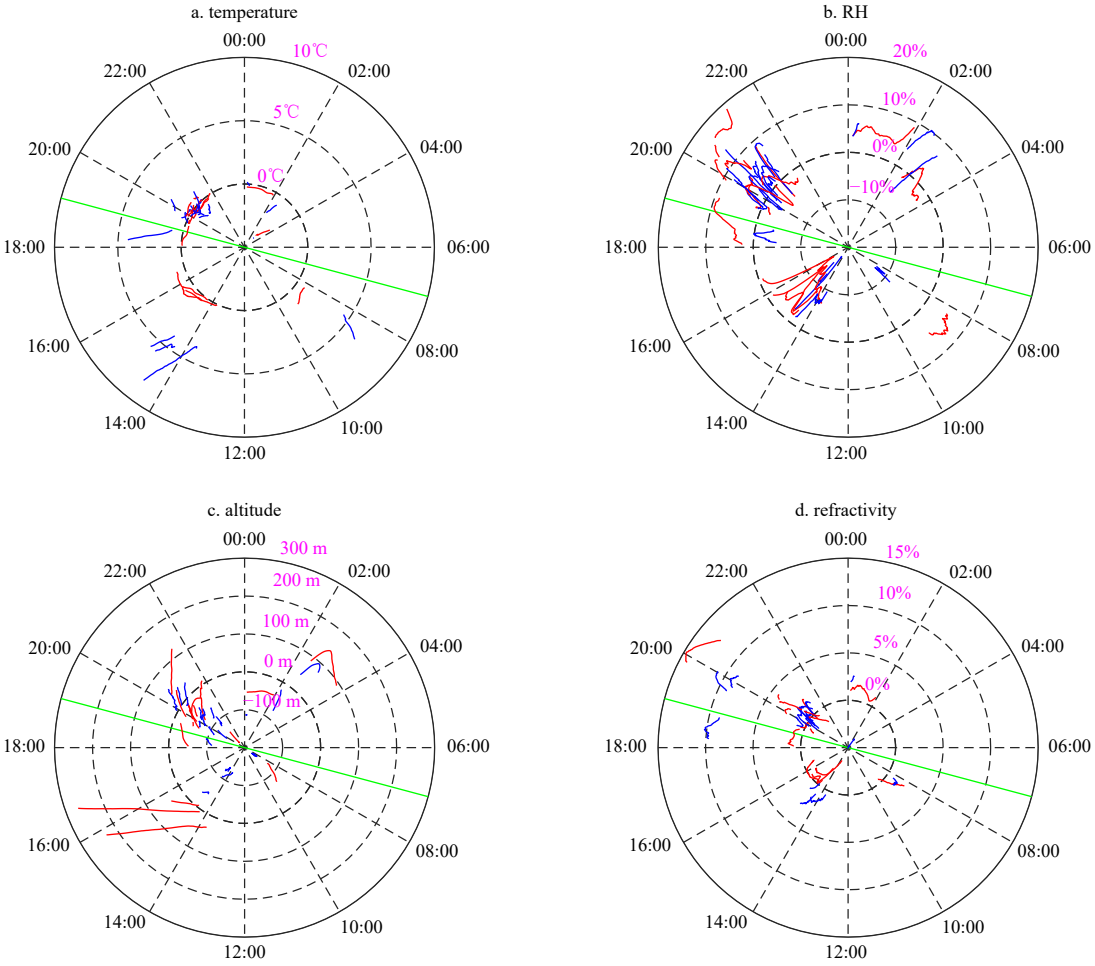

Fig. 6. Around clock biases of temperature (a), RH (b), altitude (c), and refractivity (d) derived from GPS-TK minus RS92-SGP (blue line) and CF-06-A minus RS92-SGP (red line). The green line represents the daytime and nighttime demarcation line in local time. Rose-color values represent temperature (a), RH (b), altitude (c), and refractivity (d).

shows nearly constant variation in the range of 5%–6% during daytime (Fig. 5d) and 5%–10% during nighttime (Fig. 5h), indicating the stability of the CF-06-A RH sensors during both daytime and nighttime flights. Several correction methods have been proposed to address the daytime dry bias, which may be caused by solar radiation error (e.g., Miloshevich et al., 2009; Wang et al., 2013).

3.2.3 *Around-clock biases*

In this subsection, the around-the-clock biases are examined to further investigate the time-depended biases and the errors caused by the altitude mismatch (Fig. 6). Results show a warm bias of 0.4℃ for CF-06-A and 0.5℃ for GPS-TK during daytime (06:00–20:00, local time). The temperature biases between CF-06-A and RS92-SGP are relative homogeneous (Fig. 6a), differing from the increasing biases with the altitude shown in Fig. 4c. These differences are partly due to errors of altitude mismatch (Fig. 6c). The temperature biases between GPS-TK and RS92-SGP show positive values as increasing with the time, reaching a range of 3.5–8℃, which are obviously larger than those in Fig. 4a. The discrepancy is likely due to the negative biases that inducing a false cold bias and causing the negative contributions to altitude-related errors (Fig. 6c). During the nighttime, the temperature biases are relative homogeneous with slightly negative values closed to zero for both GPS-TK and CF-06-A. During this period, the altitude biases are relatively small over the troposphere, indicating weak contributions of altitude biases to the temperature measurements of GPS-TK and CF-06-A, and longwave radiation cooling being important. Notably, one temperature measurements derived from the GPS-TK at 18:00 has a special fluctuation, with a maximum warm bias of 4.5℃ compared to RS92-SGP before sunset (local time 18:40) (Fig. 6a). This bias decreases quickly until sunset, and then the bias becomes slightly positive after sunset, indicating the negative contribution of altitude bias to the temperature bias as seen in Fig. 4e. This result suggests that the temperature sensors of GPS-TK are highly sensitive to solar radiation. For CF-06-A, the temperature is close to that of RS92-SGP, indicating good performance of temperature sensor during the daytime.

The RH biases of GPS-TK and CF-06-A show dry values during the daytime, consistent with the previous daytime results (Wang and Zhang, 2008; Sun et al., 2010). It is noteworthy that the CF-06-A measurements have moist biases around the sunrise and sunset (local 08:00 AM and 06:00 PM), which are different from the noontime (local 02:00 PM) measurements (Fig. 6b). Moist biases of around 5% are observed throughout the nighttime both in GPS-TK and CF-06-A. The qualitative agreement of RH measurements between these two types of radiosondes enhances the confidence in isolating the bias sources for daytime and nighttime.

3.3 *Corrections*

3.3.1 *Temperature corrections*

The results indicate that the temperature recorded by the GPS-TK and CF-06-A soundings are influenced by solar radiation heating, sensor infrared radiation cooling and altitude mismatch. These factors lead to discrepancies between the sensor temperature and the ambient air temperature. The GPS-TK uses a bimetal spiral band-gap thermistor to measure temperature, which lacks radiation protective shields and has uncontrollable emissivity. Consequently, it poorly reflects solar radiation and strongly absorbing and emitting infrared radiation. An analysis was conducted to establish the error characteristic of the GPS-TK associated with environmental changes. Luers and Eskridge (1995) and Luers and Eskridge (1998) performed sensitivity analysis of temperature measurements, testing the influence of various parameters on temperature error, including background temperature, pressure, humidity, cloud cover, solar angle and balloon rise rate. In this study, the reference dataset of RS92-SGP was chosen to represent the ambient atmospheric environment, and the parameters of solar angle and altitude mismatch are considered. Figure 7a shows the temperature error for GPS-TK for daytime and nighttime flights. The temperature error is significantly influenced by nighttime infrared radiation, which can result in errors up to –0.5℃. During daytime, the sonde absorbs more solar radiation at noontime, heating the sonde and enhancing the temperature error. The nighttime temperature error is less for CF-06-A (Fig. 7b) because of the low emissivity of the bead thermistor. During daytime, the temperature error of CF-06-A shows a positive trend with increasing altitude at sunrise and noontime, while at sunset, the error shows negative values due to the low solar angle. Indeed, the primary solar radiation-induced biases were identified and corrected based on the solar zenith angle for different daytime flights. However, having only one sunrise and sunset profile for daytime flights introduces uncertainty in building the correction model. This limited-sample-driven bias evaluation and correction could only be used as a reference. More inter-comparison sample should be used to address this challenge, as discussed in the discussion section.

3.3.2 *RH corrections*

The GPS-TK uses a unique capacitive sensor element for measuring RH, with calibration coefficients applied internally to calibrate the signals from the sensors. Figure 5 illustrates the major errors of the GPS-TK RH measurement in the ambient air. In this analysis, the correction algorithm for those errors is evaluated (Fig. 8a). The RH error profiles of GPS-TK are possibly related to basic calibration model error, temperature dependence correction error and altitude mismatch errors. During nighttime, the error profile shows obvious moist biases in the LT. During daytime, the error profiles show significant dry biases in the range of –10% to –20% around noontime and sunrise, while at sunset, the error profiles show slight differences within zero value versus altitude due to the low solar angle.

The RH measurement of CF-06-A radiosonde uses a capacitive thin-film humidity sensor, which has similar characteristics to the RS92-SGP. These RH sensors can take up water with reduced hysteresis and are more stable at higher humidity (Antikainen and Paukkunen, 1994). The error characteristics of RH around sunrise and sunset show a moist bias of 5% versus altitude, which is related to solar-challenging environments. The nighttime measurements show obvious moist biases in the troposphere. The error profiles of CF-06-A (Fig. 9b) are used to correct the RH measurements. Notably, the limited RH samples, especially in daytime flights, could not fully address the biases and associated calibration models in the RH profiles of GPS-TK and CF-06-A.

3.3.3 *Bias correction model development*

The correction algorithm implementation is as follows: the original temperature and RH measurements of the GPS-TK and CF-06-A (T_O and RH_O) are adjusted by subtracting the error profiles in Figs 7 and 8 ($C_T(H, D)$ and $C_{RH}(H, D)$), resulting in the corrected temperature (T_{CORR}) and RH (RH_{CORR}) given by

$$T_{CORR} = T_O - C_T(H, D), \tag{1}$$

$$RH_{CORR} = RH_O - C_{RH}(H, D), \tag{2}$$

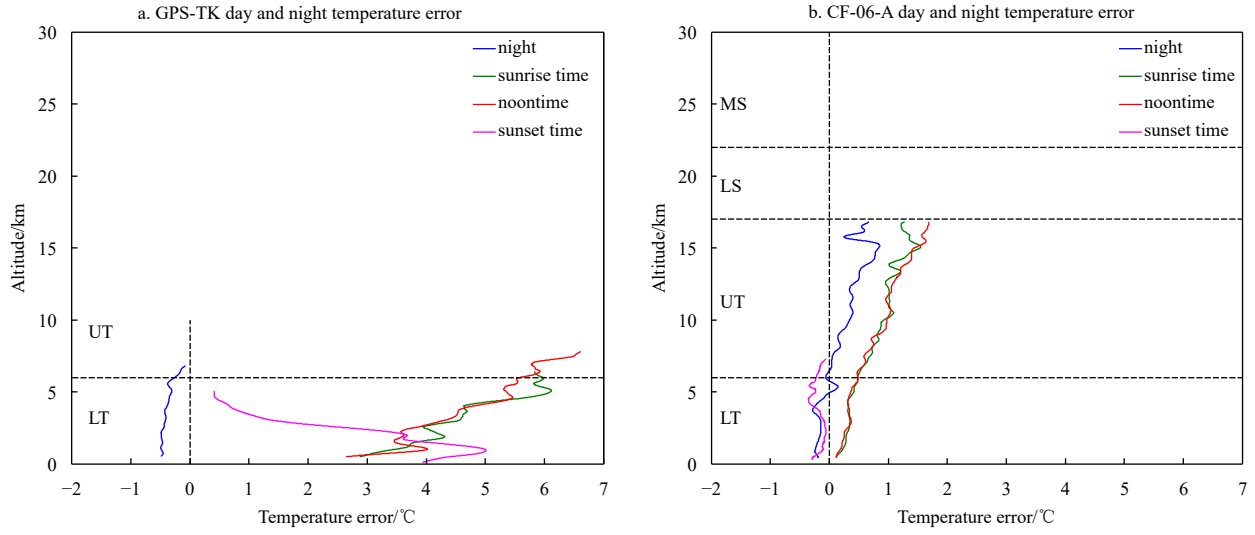

Fig. 7. Temperature errors of GPS-TK (a) and CF-06-A (b) radiosondes in daytime and nighttime. Shown are: the mean nighttime error profile (blue), the mean sunrise time profile (green), the mean noontime profile (red), and the mean sunset time profile (purple). MS: middle stratosphere; LS: lower stratosphere; UT: upper troposphere; LT: lower troposphere.

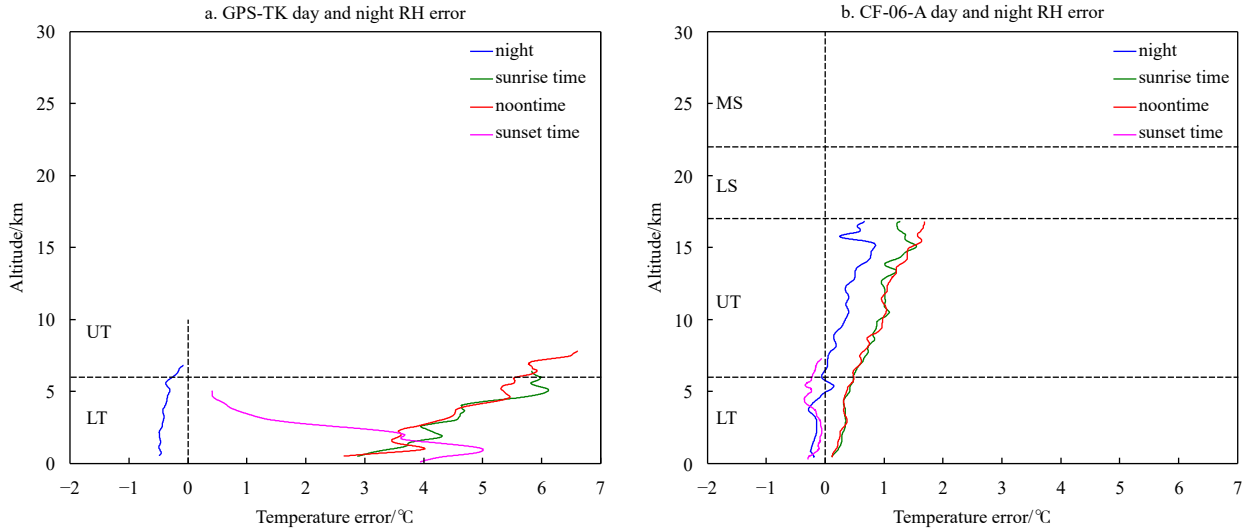

Fig. 8. RH errors of GPS-TK (a) and CF-06-A (b) radiosondes in daytime and nighttime. Shown are: the mean nighttime profile (blue), the mean sunrise-time profile (green), the mean noontime profile (red), and the mean sunset-time profile (purple). MS: middle stratosphere; LS: lower stratosphere; UT: upper troposphere; LT: lower troposphere.

where H represents the altitude and D represents the time (sunrise, sunset, noontime and nighttime). Figure 9 shows the biases of the GPS-TK/CF-06-A corrected temperature associated with the RS92-SGP during daytime and nighttime. The remaining random errors of the GPS-TK temperature measurements are within ±1.0℃ during daytime and about ±1.6℃ during nighttime. The mean biases of GPS-TK measurement are near zero both during daytime and nighttime. The RMS of GPS-TK corrected temperature during daytime remains significant, although its magnitude is smaller than that of uncorrected temperature profiles. The nighttime RMS is about 0.6℃, almost the same as the original records. These results indicate that uncertainties like sensor sensitivity, missing ground-check correction and cloud cover still affect GPS-TK soundings.

Removing the radiation effects from CF-06-A during daytime and nighttime temperature measurements yields a new bias

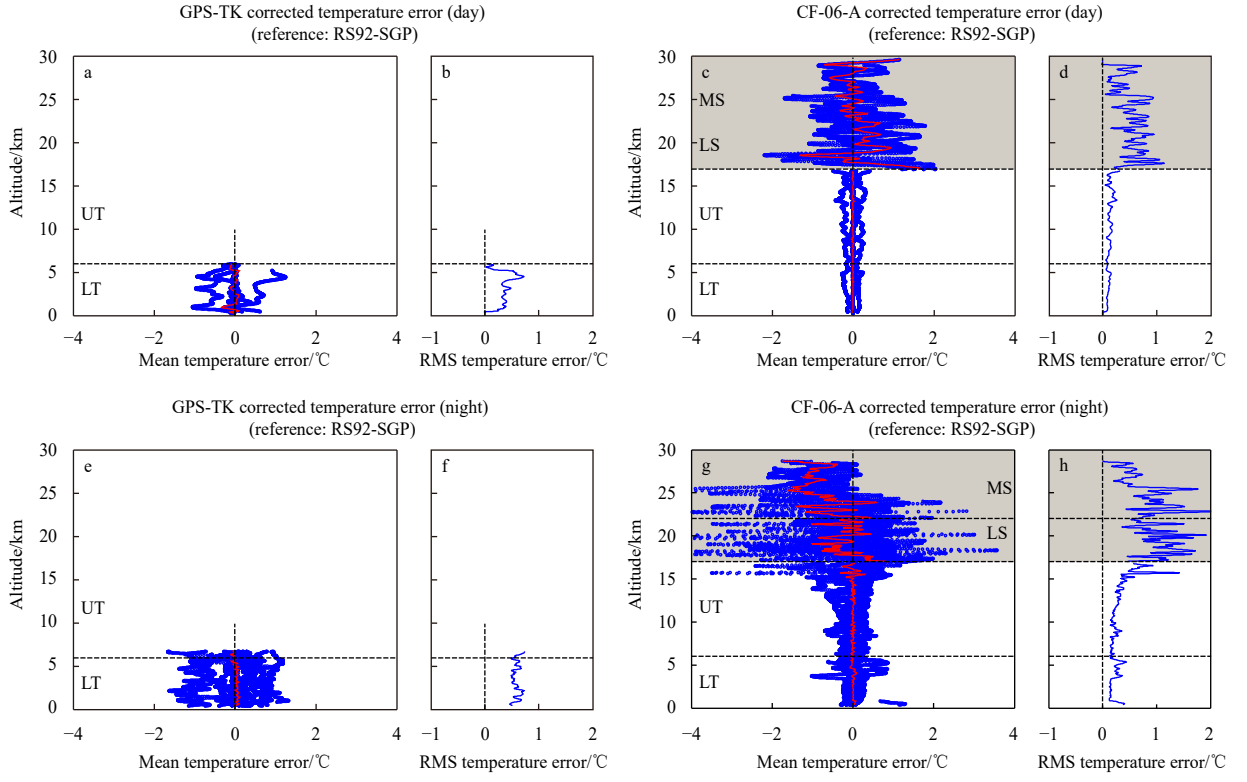

Fig. 9. Temperature errors of GPS-TK and CF-06-A corrected measurements by comparing to RS92-SGP. a and b. Mean and RMS temperature errors of corrected GPS-TK in daytime; c and d. mean and RMS temperature errors of corrected CF-06-A in daytime; e and f. mean and RMS temperature errors of corrected GPS-TK in nighttime; g and h. mean and RMS temperature errors of CF-06-A in nighttime. Red line: mean error. MS: middle stratosphere; LS: lower stratosphere; UT: upper troposphere; LT: lower troposphere.

characteristic as compared with RS92-SGP. The random temperature errors of CF-06-A during daytime are about ±0.2℃ with a slight RMS of 0.05℃ in the troposphere, while the errors fluctuate largely in the stratosphere (Fig. 9c, grey shadow). During nighttime, the errors are about ±0.4℃ in the troposphere and still fluctuate above 17 km (Fig. 9g). The results show that the residual errors preserve the random errors and that temperature measurements remain unstable in the stratosphere. The RMS of the CF-06-A corrected temperature in Figs 9d and h tends to be near zero in the troposphere.

Figure 10 shows the errors of GPS-TK and CF-06-A corrected RH by comparing them with RS92-SGP. Removing the errors yields new differences for both the GPS-TK and the CF-06-A. After the correction, the mean differences for both radiosondes are close to zero, and the RMS is smaller than that of original records for both daytime and nighttime. The results indicate that the GPS-TK and CF-06-A radiosondes suffered from significant error sources such as the basic calibration model error, temperature dependence error, and altitude mismatch error. The correction implementation greatly contributes to reducing these error sources. However, due to a lack of reliable reference measurements, there remain obvious random errors in CF-06-A and GPS-TK. Other error sources, like chemical contamination error, sensor-arm-heating error, ground-check error and sensor aging error (<0.5% RH/a), are still unresolved.

3.4 *Application of corrections to historical records and validation*

3.4.1 *Corrections of GPS-TK historical records*

The above correction algorithms were applied to the GPS-TK historical records, and their accuracy was further quantified by comparing them with the collocated COSMIC data. COSMIC measurement occurring within 3 h and 400 km of radiosonde releases from 2006 to 2012 were used for this comparison. In total, there were 45 daytime matches and 36 nighttime matches. Each GPS-TK historical record was interpolated to a 100 m interval and visually inspected for reasonableness before comparison. The results indicated that all matched soundings passed the completeness check with high quality. Figures 11 and 12 illustrate the temperature and RH measurements for both daytime and nighttime. Before correction, the temperature biases of GPS-TK exhibited anomalously large deviations (from 1℃ to 7℃ at the surface to over 10℃ in the upper troposphere) and a daytime RMS error of 1.5℃, reflecting significant solar radiation heating errors in the GPS-TK historical daytime dataset. After corrections, most warm biases were removed and the remaining errors converge to relative homogeneity (averaging about 2℃). The difference in RMS before and after corrections was approximately 0.05℃. For nighttime, the effect of the correction was weaker due to the persistent warm biases, differing from the results compared with RS92-SGP. This discrepancy likely arises from the impacts of the time and distance mismatch between COSMIC and radiosonde (Sun et al., 2010).

Application of the correction algorithms to the GPS-TK historical RH records also improved their accuracy for both during daytime and nighttime (Fig. 12). Before correction, the GPS-TK RH measurements showed a dry bias increasing with altitude from –6% to –22% during daytime. After correction, the mean bias reduced to –10% at most levels. During nighttime, the correction effected on GPS-TK RH measurements was less clear. As seen in Figs 5e and 13e, the GPS-TK RH biases derived from COSMIC differed significantly from those derived from Vaisala RS92-

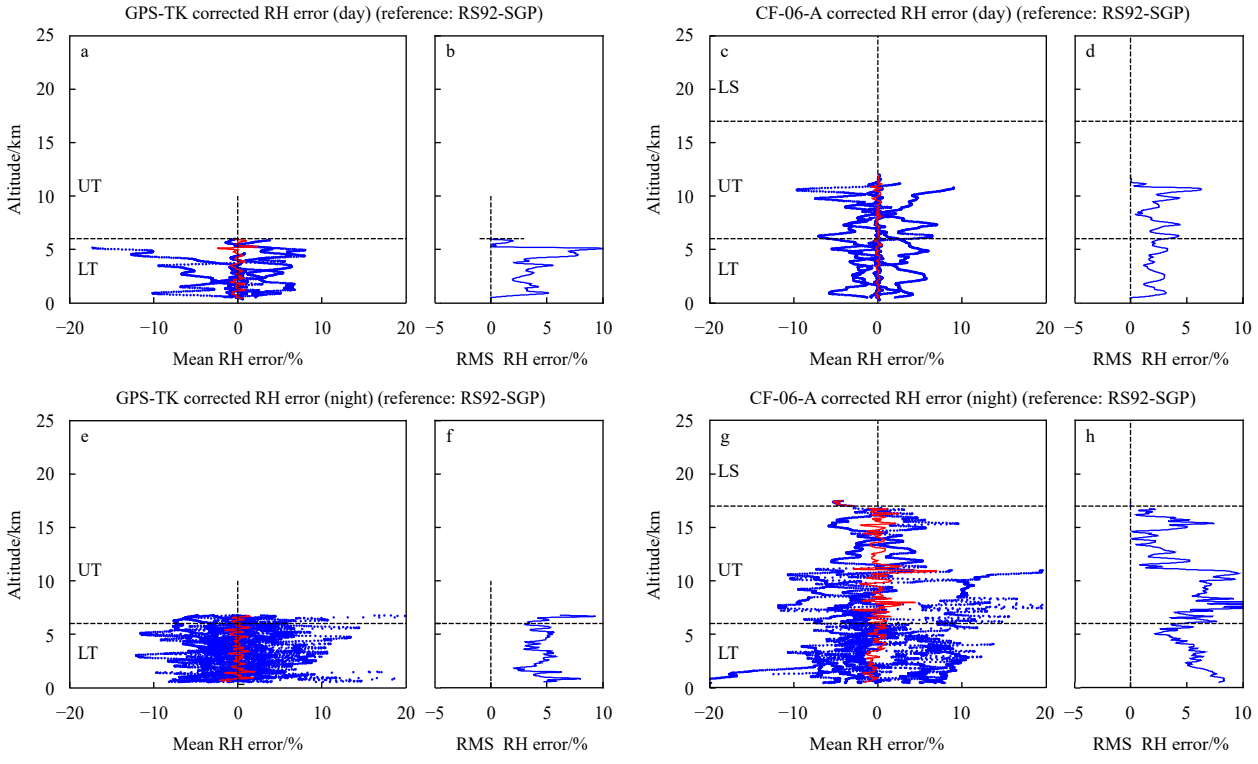

Fig. 10. RH errors of GPS-TK and CF-06-A corrected measurements by comparing to RS92-SGP. a and b. Mean and RMS RH errors of corrected GPS-TK in daytime; c and d. mean and RMS RH errors of corrected CF-06-A in daytime; e and f. mean and RMS RH errors of corrected GPS-TK in nighttime; g and h. mean and RMS RH errors of CF-06-A in nighttime. Red line: mean error. LS: lower stratosphere; UT: upper troposphere; LT: lower troposphere.

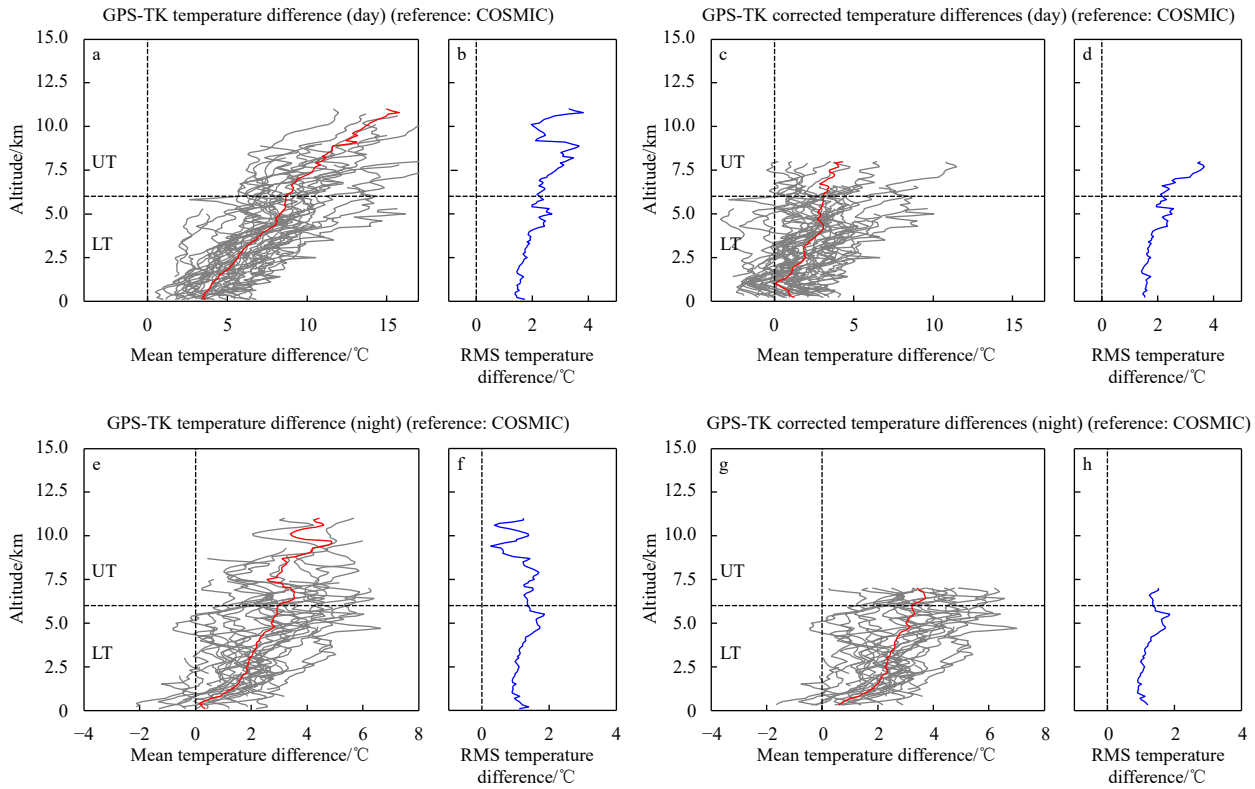

Fig. 11. Inter-comparison of GPS-TK historical records with COSMIC temperature measurements before and after correction. a and b. Mean and RMS temperature differences of GPS-TK in daytime before correction; c and d. mean and RMS temperature differences of GPS-TK in daytime after correction; e and f. mean and RMS temperature differences of GPS-TK in nighttime before correction; g and h. mean and RMS temperature differences of GPS-TK in nighttime after correction. Gray lines in a, c, e, and g are the individual temperature differences for each inter-comparison. The collocation of COSMIC is 3 h and 400 km. UT: upper troposphere; LT: lower troposphere.

SGP during nighttime. This discrepancy is likely associated with the COSMIC vapor pressure convertion from refractivity.

After the correction, the GPS-TK historical radiosonde records showed gratifying improvements, with smaller and more stable biases and a reduced influence of radiation effects.

3.4.2 *Validation*

After applying corrections, each radiosonde sounding was examined for "reasonableness" by analyzing the Atmospheric Boundary Layer Height (ABLH), Convective Available Potential Energy (CAPE) and Convective Inhibition (CIN). Figure 13 shows the ABLH from 20 simultaneous radiosonde records before and after corrections during daytime and nighttime. Before corrections, the ABLH derived from GPS-TK showed significant differences, with a mean value of 700 m. After corrections, the ABLH variations range of 800–1 000 m for GPS-TK and CF-06-A during daytime (Fig. 13b), which aligns more closely with RS92-SGP expectations for marine tropical environments. Figures 13c and d indicate that the variations in GPS-TK and CF-06-A measurements are similar to those of RS92-SGP before and after corrections during nighttime, suggesting that the ABLH derived from GPS-TK and CF-06-A is minimally influenced by temperature and RH corrections during nighttime.

Figure 14 shows histograms of CAPEs and CINs before and after corrections. CAPEs are calculated from temperature, RH and pressure profiles up to an altitude of 6 000 m. The majority (54.82%) of corrected GPS-TK soundings have CAPE values above 300 J/kg during June, July and August (JJA), which represents a 40% increase over uncorrected soundings (Fig. 14a). Generally, CAPE values over the marine tropical environment are sufficient for convective initiation, with values derived from NCEP reanalysis in JJA reaching 1 002.5 J/kg. These corrected soundings appear "reasonable" with high values and percentages of CAPEs. The dry biases in RH measurements might be a key reason for the weak CAPEs within uncorrected sounding records (Lucas and Zipser, 2000; Guichard et al., 2000; Wang et al., 2002; Xie et al., 2014). The features of the CIN were also evaluated (Fig. 14b). Results show that the CIN derived from the corrected GPS-TK profiles correspond well with the NCEP reanalysis data (average value 37.4 J/kg in JJA over the SCS), with reasonable magnitude and proper percentage (Fig. 14b).

4 Summary and discussion

The biases in the historical temperature and RH radiosonde records have been revealed by through comparisons with COSMIC RO, leading to an unrealistic marine atmospheric environment for scientific applications. Based on the simultaneous inter-comparison, the error characteristics of GPS-TK and CF-06-A radiosondes have been examined, and a correction methodology has been developed to correct the historical radiosonde records.

The mean temperature biases of GPS-TK show a warm bias of 2℃ near surface to a predominant warm bias of 6℃ in the upper troposphere during daytime and a notable cool bias (about –0.5℃) with an RMSE of 0.8℃ in the lower level (below 7 km) during nighttime. For RH inter-comparisons, the GPS-TK indicates a dry mean bias of –10% during daytime and a moist bias of

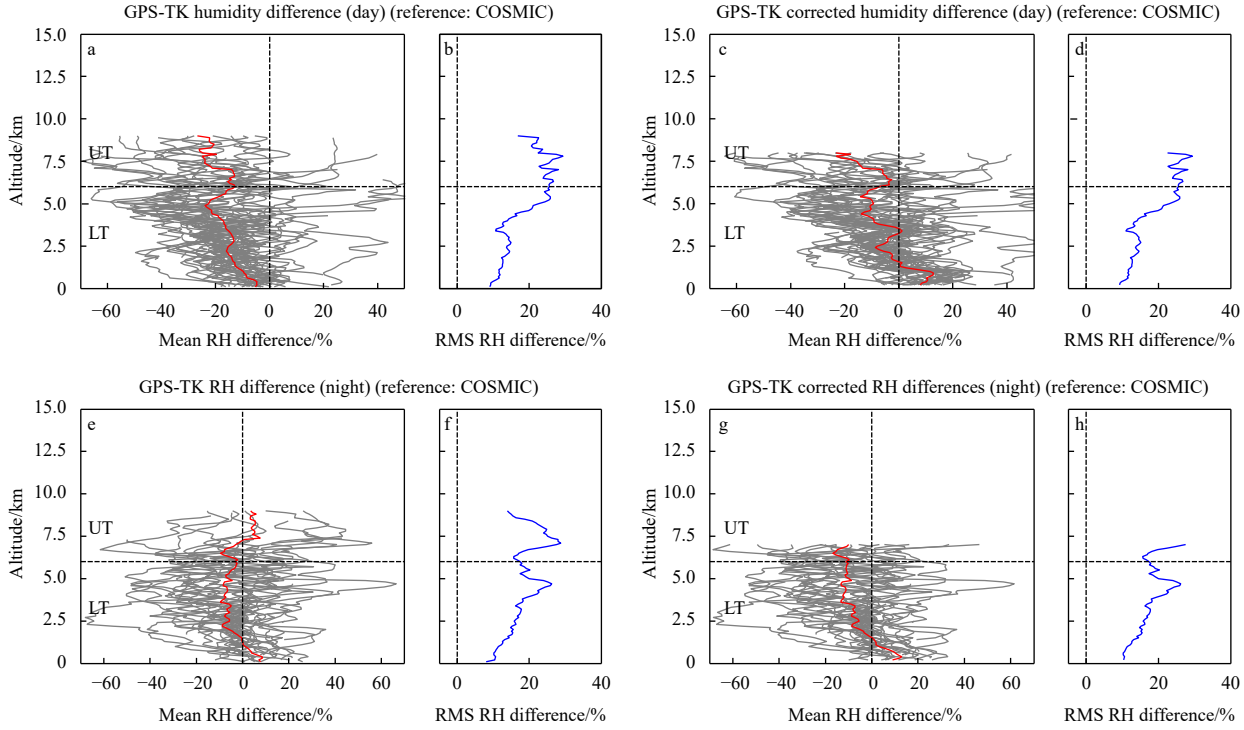

Fig. 12. Inter-comparison of GPS-TK historical records with COSMIC RH measurements before and after correction. a and b. Mean and RMS RH differences of GPS-TK in daytime before correction; c and d. mean and RMS RH differences of GPS-TK in daytime after correction; e and f. mean and RMS RH differences of GPS-TK in nighttime before correction; g and h. mean and RMS of GPS-TK RH differences in nighttime after correction. Gray lines in a, c, e, and g are the individual RH differences for each inter-comparison. The collocation of COSMIC is 3 h and 400 km. UT: upper troposphere; LT: lower troposphere.

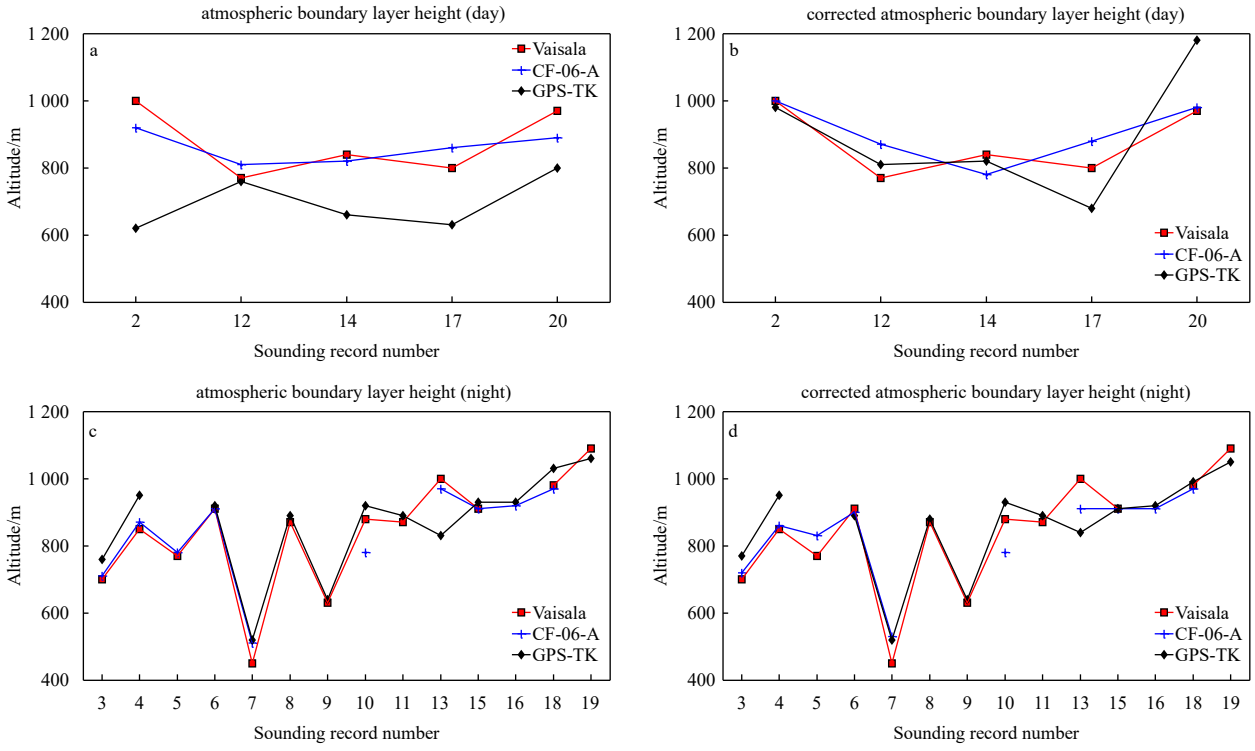

Fig. 13. Atmospheric boundary layer height derived from RS92-SGP (red), GPS-TK (black) and CF-06-A (blue) in daytime (a, b) and nighttime (c, d) flights. Horizontal ordinate represents the release sample number. a and c are derived from measurements before corrections; b and d are after corrections.

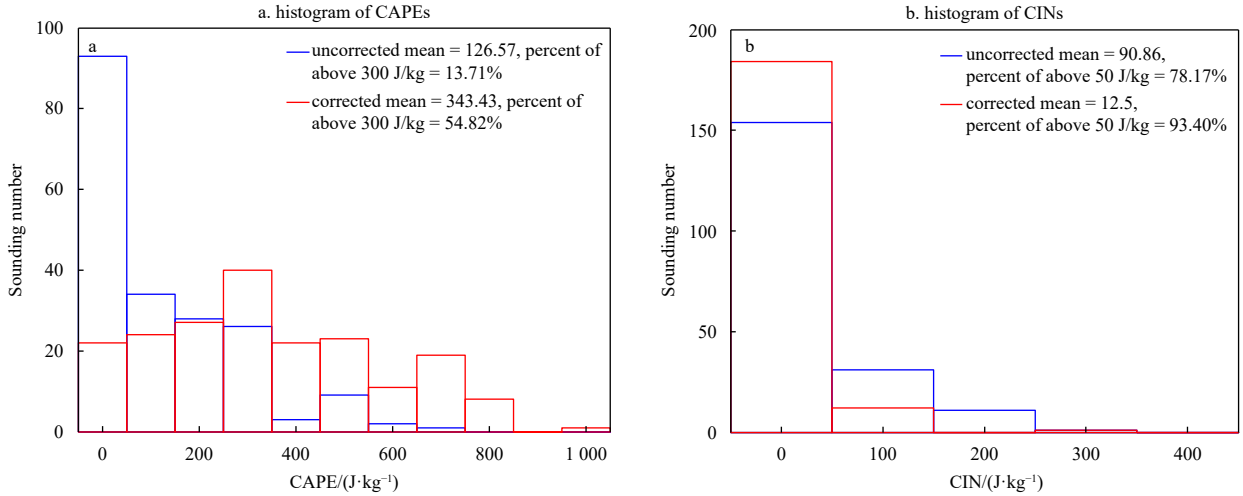

Fig. 14. Histograms of CAPEs (a) and CINs (b) derived from GPS-TK historical soundings during the JJA (June, July and August, 2006–2011) before (blue) and after (red) corrections.

6% during nighttime. The daytime inter-comparisons of the CF-06-A with the RS92-SGP show that the temperature has a warm bias which increases with altitude within 1℃ in the upper troposphere and varying greatly in the stratosphere. During nighttime, the mean temperature biases change from a cool bias of –0.4℃ below 12 km to a warm bias in the upper troposphere. The RH shows a dry bias of 2%–4% during daytime and a moist bias in the range of 4%–8% during nighttime throughout the troposphere. The GPS-TK exhibits relatively larger errors both during daytime and nighttime compared to CF-06-A, indicating pronounced radiation effects. Around-clock biases denote that the altitude mismatch significantly influences the temperature and RH measurements in both CF-06-A and GPS-TK.

An empirical correction derived from this inter-comparison is applied to remove the radiation-dependence and altitude mismatch errors in GPS-TK and CF-06-A. The corrected temperature and RH profiles align well with those obtained from the RS92-SGP, except for the stratosphere measurements of CF-06-A due to strong random errors. The correction algorithms are applied to the GPS-TK historical radiosonde records and the corrected results are verified by comparing with the COSMIC. After corrections, significant improvements are observed within the GPS-TK historical radiosonde records, showing smaller biases and a weak influence of radiation effects. The corrected temperature and RH profiles are generally reasonableness in reflecting the realistic marine atmospheric environment. Before corrections, the ABLH calculated from daytime soundings exhibited significant errors with low values, which are related to the temperature bias. The dry RH biases in GPS-TK humidity data contribute to low CAPEs and large CINs in uncorrected sounding records. After corrections, there are substantial improvements in the magnitude and intensity percentage of ABLH, CAPEs and CINs.

However, there are importance caveats to consider. For daytime soundings, clouds can affect solar radiation error in very complicated ways, making daytime error correction unreliable (Luers, 1997). Clouds do not affect the nighttime results. Additionally, the above correction algorithm does not consider the sonde age, which can introduce errors due to unstable drifts during the storage (Wang et al., 2002). The basic calibration model of CF-06-A in the stratosphere is generally considered “unreasonable” and further confirmation of error characteristics is needed.

One uncertainty in our correction algorithm implementation is the small sample size of shipboard simultaneous inter-comparison soundings. The five daytime flights were utilized as a group under one bias source of solar zenith angle by considering different launched times of sunrise, noon, and sunset. Indeed, having only one sunrise and sunset profile for daytime flights introduces significant uncertainty in building the correction model. This limited-sample-driven bias evaluation and correction during sunrise and sunset profiles could only be used as a reference. The limitations of shipboard less simultaneous inter-comparison sounding make it challenging to understand the uncertainties and sensitivities of soundings along with different errors. To address the challenge of limited samples, we propose establishing an environment simulation laboratory that accurately simulates the oceanic atmosphere and performs traceable calibrations. This will help improve the limitations of shipboard simultaneous inter-comparison soundings in this study. We intend to build a system of calibration probes to validate the temperature and RH probes of GPS-TK and CF-06-A, similar to the approach by Miloshevich et al. (2009). These probes’ accuracies will be well characterized as a function of height, RH, thermal lag and time of day (or solar zenith angle) through large-sample laboratory experiments.

Acknowledgements

This work would not have been possible without the excellent work of the crews and technicians of the R/V *ShiYan 1*. In particular, the authors thank Yeqiang Shu, Ju Chen, Qinyan Liu, Yukun Qian, Xiaofeng Zhao and Jinggen Xiao for discussions. This study is supported by the High-Performance Computing Division and HPC managers of Wei Zhou and Dandan Sui in the South China Sea Institute of Oceanology. COSMIC RO data are openly available at https://www.cosmic.ucar.edu/. NCEP data analyzed in this study were a re-analysis of existing data, which are openly available at NCEP/NCAR Reanalysis 1: NOAA Physical Sciences Laboratory. Further information about these data and conditions for access are available at the Yang et al. (2015) at doi: 10.1175/BAMS-D-14-00159.1 and South China Sea Ocean Data Center (https://data.scsio.ac.cn/).

References

Angling M. 2016. ROM SAF CDOP-2 visiting scientist report 28: A new software tool for reducing systematic residual ionospheric

errors in GNSS-RO level 3 products. https://rom-saf.eumetsat.int/Publications/reports/romsaf_vs28_rep_v10.pdf [2016-12-16]
Antikainen V, Paukkunen A. 1994. Studies on improving humidity measurements in radiosondes. In: Proceedings of WMO Tech. Conference on Instruments and Methods of Observation. Geneva, Switzerland, WMO: 137–141
Balagurov A, Kats A, Krestyannikova N, et al. 2006. WMO Radiosonde Humidity Sensor Intercomparison: final report of Phase I and Phase II. In: Instruments and Observing Methods Report No. 85, WMO/TD-No. 1305, Geneva, Switzerland: WMO, https://library.wmo.int/records/item/35357-twmo-radiosonde-humidity-sensor-intercomparison-final-report-of-phase-i-and-phase-ii
Baldwin M P, Gray L J, Dunkerton T J, et al. 2001. The quasi-biennial oscillation. Reviews of Geophysics, 39(2): 179–229, doi: 10.1029/1999RG000073
Chang Liang, Guo Lixin, Feng Guiping, et al. 2018. Comparison of the Arctic upper-air temperatures from radiosonde and radio occultation observations. Acta Oceanologica Sinica, 37(1): 30–39, doi: 10.1007/s13131-018-1156-x
Cheng Yinhe, Zhou Shengqi, Wang Dongxiao, et al. 2015. Statistical characteristics of the surface ducts over the South China Sea from GPS radiosonde data. Acta oceanologica sinica, 34(11): 63–70, doi: 10.1007/s13131-015-0749-x
Da Silveira, Fisch R G, Machado L, et al. 2006. WMO Intercomparison of GPS Radiosondes, Alcantara, Brazil, 2001. Geneva: WMO
Durre I, Vose R S, Wuertz D B. 2006. Overview of the integrated global radiosonde archive. Journal of Climate, 19(1): 53–68, doi: 10.1175/JCLI3594.1
Eisenman I, Yu Lisan, Tziperman E. 2005. Westerly wind bursts: ENSO's tail rather than the dog?. Journal of Climate, 18(24): 5224–5238
Goff J A, Gratch S. 1946. Low-pressure properties of water from –160 to 212 °F. In: Transactions of the American Society of Heating and Ventilating Engineers. New York, NY, USA: American Society of Heating, Refrigeration and Air Conditioning Engineers, Inc., 52: 95–122.
Guichard F, Parsons D, Miller E. 2000. Thermodynamic and radiative impact of the correction of sounding humidity bias in the tropics. Journal of Climate, 13(20): 3611–3624, doi: 10.1175/1520-0442(2000)013<3611:TARIOT>2.0.CO;2
He Wenying, Ho S P, Chen Hongbin, et al. 2009. Assessment of radiosonde temperature measurements in the upper troposphere and lower stratosphere using COSMIC radio occultation data. Geophysical Research Letters, 36(17): L17807, doi: 10.1029/2009GL038712
Ho S P, Goldberg M, Kuo Ying-Hwa, et al. 2009. Calibration of temperature in the lower stratosphere from microwave measurements using COSMIC radio occultation data: preliminary results. Terrestrial, Atmospheric and Oceanic Sciences, 20(1): 87–100, doi: 10.3319/TAO.2007.12.06.01(F3C)
Hooper A H. 1986. WMO international radiosonde comparison. Phase I: Beaufort Park, UK, 1984. Geneva, Swizerland: WMO, 118
Ivanov A, Kats S, Kurnosenko S, et al. 1991. WMO international radiosonde comparison. Phase III: Dzhambul, USSR, 1989. Geneva: WMO, 135
Jauhiainen H, Lehmuskero M, Åkerberg J. 2005. Vaisala RS92 Radiosondes offer a high level of GPS performance with a reliable telemetry link. TECO 2005 Bucharest, https://www.sigidwiki.com/images/5/5c/Vaisala_RS92_Radiosondes_Presentation.pdf [2005-05-05]
Kuo Y H, Schreiner W S, Wang J, et al. 2005. Comparison of GPS Radio occultation soundings with radiosondes. Geophysical Research Letters, 32(5): L05817, doi: 10.1029/2004GL021443
Li Wei, Zhao Peitao, Guo Qiyun, et al. 2011. The international radiosonde intercomparison results for China-made GPS radiosonde. Journal of Applied Meteorological Science (in Chinese), 22(4): 453–462
Lucas C, Zipser E J. 2000. Environmental variability during TOGA COARE. Journal of the Atmospheric Sciences, 57(15): 2333–2350, doi: 10.1175/1520-0469(2000)057<2333:EVDTC>2.0.CO;2
Luers J K. 1997. Temperature error of the Vaisala RS90 radiosonde. Journal of Atmospheric and Oceanic Technology, 14(6): 1520–1532, doi: 10.1175/1520-0426(1997)014<1520:TEOTVR>2.0.CO;2
Luers J K, Eskridge R E. 1995. Temperature corrections for the VIZ and Vaisala radiosondes. Journal of Applied Meteorology, 34(6): 1241–1253, doi: 10.1175/1520-0450(1995)034<1241:TCFTVA>2.0.CO;2
Luers J K, Eskridge R E. 1998. Use of radiosonde temperature data in climate studies. Journal of Climate, 11(5): 1002–1019, doi: 10.1175/1520-0442(1998)011<1002:UORTDI>2.0.CO;2
Mclnturff R M, Finger F G, Johnson K W, et al. 1979. Day-night differences in radiosonde observations of the stratosphere and troposphere. NOAA technical memorandum NWS NMC, 63, https://repository.library.noaa.gov/view/noaa/55700
Meehl G A. 1997. The South Asian monsoon and the tropospheric biennial oscillation. Journal of Climate, 10(8): 1921–1943, doi: 10.1175/1520-0442(1997)010<1921:TSAMAT>2.0.CO;2
Miloshevich L M, Vömel H, Paukkunen A, et al. 2001. Characterization and correction of relative humidity measurements from Vaisala RS80-A radiosondes at cold temperatures. Journal of Atmospheric and Oceanic Technology, 18(2): 135–156, doi: 10.1175/1520-0426(2001)018<0135:CACORH>2.0.CO;2
Miloshevich L M, Vömel H, Whiteman D N, et al. 2009. Accuracy assessment and correction of Vaisala RS92 radiosonde water vapor measurements. Journal of Geophysical Research: Atmospheres, 114(D11): D11305, doi: 10.1029/2008JD011565
Nash J, Oakley T, Vömel H, et al. 2011. WMO intercomparison of high quality radiosonde system. Geneva, Swizerland: WMO
Nash J, Schmidlin F J. 1987. WMO international radiosonde comparison (U.K. 1984, U.S.A. 1985). Geneva, Swizerland: WMO, 103
Nash J, Smout R, Oakley T, et al. 2006. WMO intercomparison of radiosonde systems, Vacoas, Mauritius, 2-25 February 2005. In: Instruments and Observing Methods Report No. 83: The WMO Intercomparison of Radiosonde Systems: final report. Geneva, Switzerland: WMO, https://library.wmo.int/records/item/35338-the-wmo-intercomparison-of-radiosonde-systems-final-report
Peng Shiqiu, Zhu Yuhang, Huang Ke, et al. 2016. Detecting the structure of marine atmospheric boundary layer over the Northern South China Sea by shipboard GPS sondes. Atmospheric Science Letters, 17(10): 564–568, doi: 10.1002/asl.693
Qin Z, Zou X, Weng F. 2012. Comparison between linear and nonlinear trends in NOAA-15 AMSU-A brightness temperatures during 1998–2010. Climate Dynamics, 39(7): 1763–1779
Schmidlin F J. 1988. WMO international radiosonde intercomparison. Phase II, 1985, Wallops Island, Virginia USA. Geneva, Swizerland: WMO, 113
Seidel D J, Angell J K, Christy J, et al. 2004. Uncertainty in signals of large-scale climate variations in radiosonde and satellite upper-air temperature datasets. Journal of Climate, 17(11): 2225–2240, doi: 10.1175/1520-0442(2004)017<2225:UISOLC>2.0.CO;2
Shi Rui, Chen Ju, Guo Xinyu, et al. 2017. Ship observations and numerical simulation of the marine atmospheric boundary layer over the spring oceanic front in the northwestern South China Sea. Journal of Geophysical Research: Atmospheres, 122(7): 3733–3753, doi: 10.1002/2016JD026071
Sinha P R, Sahu L K, Manchanda R K, et al. 2016. Transport of tropospheric and stratospheric ozone over India: balloon-borne observations and modeling analysis. Atmospheric Environment, 131: 228–242, doi: 10.1016/j.atmosenv.2016.02.001
Sun Bomin, Reale A, Seidel D J, et al. 2010. Comparing radiosonde and COSMIC atmospheric profile data to quantify differences among radiosonde types and the effects of imperfect collocation on comparison statistics. Journal of Geophysical Research: Atmospheres, 115(D23): D23104, doi: 10.1029/2010JD014457
Suortti T M, Kivi R, Kats A, et al. 2008. Tropospheric comparisons of vaisala radiosondes and balloon-borne frost-point and lyman-α hygrometers during the LAUTLOS-WAVVAP Experiment. Journal of Atmospheric and Oceanic Technology, 25(2): 149–

166, doi: 10.1175/2007JTECHA887.1

Tian Xiaoxu, Zou Xiaolei. 2020. Comparison of advanced technology microwave sounder biases estimated using radio occultation and hurricane Florence (2018) captured by NOAA-20 and S-NPP. Advances in Atmospheric Sciences, 37(3): 269–277, doi: 10.1007/s00376-019-9119-5

Vömel H, Oltmans S J, Johnson B J, et al. 2002. Balloon-borne observations of water vapor and ozone in the tropical upper troposphere and lower stratosphere. Journal of Geophysical Research: Atmospheres, 107(D14): 4210, doi: 10.1029/2001JD000707

Vömel H, Selkirk H, Miloshevich L, et al. 2007. Radiation dry bias of the vaisala RS92 humidity sensor. Journal of Atmospheric and Oceanic Technology, 24(6): 953–963, doi: 10.1175/JTECH2019.1

Wang Lei, Bao Qing, Li Jinxiao, et al. 2019. Comparisons of the temperature and humidity profiles of reanalysis products with shipboard GPS sounding measurements obtained during the 2018 Eastern Indian Ocean Open Cruise. Atmospheric and Oceanic Science Letters, 12(3): 177–183, doi: 10.1080/16742834.2019.1588065

Wang Junhong, Cole H L, Carlson D J, et al. 2002. Corrections of humidity measurement errors from the vaisala RS80 radiosonde-application to TOGA COARE data. Journal of Atmospheric and Oceanic Technology, 19(7): 981–1002, doi: 10.1175/1520-0426(2002)019<0981:COHMEF>2.0.CO;2

Wang Junhong, Zhang Liangying. 2008. Systematic errors in global radiosonde precipitable water data from comparisons with ground-based GPS measurements. Journal of Climate, 21(10): 2218–2238, doi: 10.1175/2007JCLI1944.1

Wang Junhong, Zhang Liangying, Dai Aiguo, et al. 2013. Radiation dry bias correction of Vaisala RS92 humidity data and its impacts on historical radiosonde data. Journal of Atmospheric and Oceanic Technology, 30(2): 197–214, doi: 10.1175/JTECH-D-12-00113.1

Wang Jin, Zhang Jie, Fan Chenqing, et al. 2014. Validation of the "HY-2" altimeter wet tropospheric path delay correction based on radiosonde data. Acta Oceanologica Sinica, 33(5): 48–53, doi: 10.1007/s13131-014-0473-y

Wang Dongxiao, Zhou Wen, Yu Xiaoli, et al. 2010. Marine atmospheric boundary layers associated with summer monsoon onset over the South China Sea in 1998. Atmospheric and Oceanic Science Letters, 3(5): 263–270, doi: 10.1080/16742834.2010.11446880

Xie Qiang, Huang Ke, Wang Dongxiao, et al. 2014. Intercomparison of GPS radiosonde soundings during the eastern tropical Indian Ocean experiment. Acta Oceanologica Sinica, 33(1): 127–134, doi: 10.1007/s13131-014-0422-9

Yagi S, Mita A, Inoue N. 1996. WMO international radiosonde comparison. Phase IV: Tsukuba, Japan, 15 February–12 March 1993. Geneva, Swizerland: WMO, 129

Yang Lei, Wang Dongxiao, Huang Jian, et al. 2015. Toward a mesoscale hydrological and marine meteorological observation network in the South China Sea. Bulletin of the American Meteorological Society, 96(7): 1117–1135, doi: 10.1175/BAMS-D-14-00159.1

Yao Wen, Ma Ying, Gao Lina. 2017. Comparison of relative humidity data between L-band and 59–701 sounding system. Journal of Applied Meteorological Science (in Chinese), 28(2): 218–226

Yoneyama K, Fujita M, Sato N, et al. 2008. Correction for radiation dry bias found in RS92 radiosonde data during the MISMO field experiment. Sola, 4: 13–16, doi: 10.2151/sola.2008-004

Yu Xiaoli, Xie Qiang, Wang Dongxiao. 2009. Diurnal cycle of marine atmospheric boundary layer during the 1998 summer monsoon onset over South China Sea. Journal of Tropical Oceanography (in Chinese), 28(2): 31–35

Yunck T P, Fetzer E J, Mannucci A M, et al. 2009. Use of radio occultation to evaluate atmospheric temperature data from spaceborne infrared sensors. Terrestrial, Atmospheric and Oceanic Sciences, 20(1): 71–85, doi: 10.3319/TAO.2007.12.08.01(F3C)

Zhai Panmao, Eskridge R E. 1996. Analyses of inhomogeneities in radiosonde temperature and humidity time series. Journal of Climate, 9(4): 884–894, doi: 10.1175/1520-0442(1996)009<0884:AOIIRT>2.0.CO;2

Zhang Weixing, Lou Yidong, Cao Yunchang, et al. 2019. Corrections of radiosonde-based precipitable water using ground-based GPS and applications on historical radiosonde data over China. Journal of Geophysical Research: Atmospheres, 124(6): 3208–3222, doi: 10.1029/2018JD029662

Zou Xiaolei, Liu Hui, Kuo Ying-Hwa. 2019. Occurrence and detection of impact multipath simulations of bending angle. Quarterly Journal of the Royal Meteorological Society, 145(721): 1690–1704, doi: 10.1002/qj.3520

Zou Xiaolei, Tian Xiaoxu. 2018. Hurricane warm-core retrievals from AMSU-A and remapped ATMS measurements with rain contamination eliminated. Journal of Geophysical Research: Atmospheres, 123(19): 10815–10829, doi: 10.1029/2018JD028934

Appendix: Reconstructed formula of atmospheric pressure and validation

Based on the temperature, RH and altitude profiles derived from the GPS radiosonde sounding, the atmospheric pressure is calculated as follows. For the given parameters P_1, T_1, RH_1, and H_1 in the first layer and T_2, RH_2, and H_2 in the second layer (Fig. A1), Eq. (A1) is used to calculate the P_2 in the second layer:

$$P_2 = P_1 \cdot \exp\left(-\frac{\Delta H}{18\,410.01 \times \frac{\overline{T}_\mathrm{V}}{273.15}}\right), \tag{A1}$$

where P_1 is the first layer pressure (hPa), P_2 is the second layer pressure (hPa). ΔH is the thickness between the first and second layers, $\Delta H = H_2 - H_1$ (unit: m); $\overline{T}_V$ is the mean virtual potential temperature between the first and second layers. The mean virtual potential temperature is calculated as follows:

$$\overline{T}_\mathrm{V} = \overline{T} \cdot (1 + 0.378\,\overline{e}/\overline{P}), \tag{A2}$$

where $\overline{T}$ is the mean temperature between the first and second layers, $\overline{T} = T_2 - T_1$ (unit: K); $\overline{e}$ is the mean vapor pressure between the first and second layers (unit: hPa). The mean vapor pressure is calculated from the Goff-Gratch equation (Goff and Gratch, 1946) based on the $\overline{\mathrm{RH}}$ and temperature $\overline{T}$, where $\overline{\mathrm{RH}} = \mathrm{RH}_2 - \mathrm{RH}_1$, $\overline{T} = T_2 - T_1$.

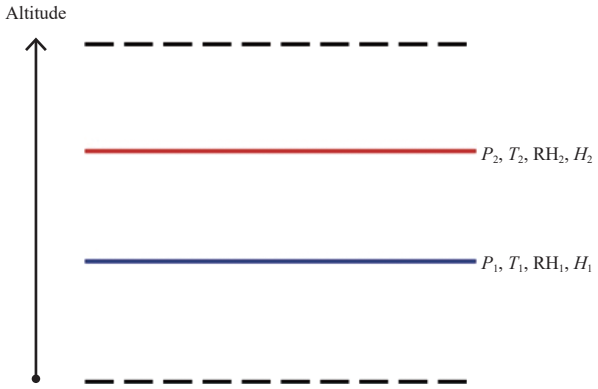

Fig. A1. Schematic showing the stratified structure of atmospheric parameter in calculating the pressure.

Figure A2 shows the atmospheric pressure profile derived from RS92-SGP and the back-calculated pressure based on the temperature and RH profiles derived from the same sounding. The results show that the reconstructed pressure profile consistent with the sounding output very well in the troposphere, within a barely bias of 2 hPa. However, the biases show with a significant value of +15 hPa in the stratosphere, indicating the poor performance of black-calculated equation and lack of vapor pressure due to the extremely cold and dry condition. The reconstructed formula is major applied to fill the missing pressure values, especially for GPS-TK sounding that with no pressure output.

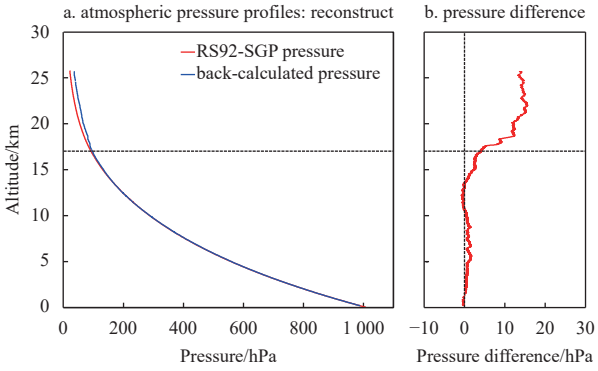

Fig. A2. Pressure profile derived from direct measurements of RS92-SGP (red line) and the reconstructed pressure profile derived from RS92-SGP temperature and RH measurements (blue line) (a), and their biases (b).